Electric field control of the LaAlO3/SrTiO3 interface ground state

A. D. Caviglia, S. Gariglio, N. Reyren, D. Jaccard, T. Schneider, M. Gabay, Stefan Thiel, German Hammerl, Jochen Mannhart, Jean-Marc Triscone

Angaben zur Veröffentlichung / Publication details:

Caviglia, A. D., S. Gariglio, N. Reyren, D. Jaccard, T. Schneider, M. Gabay, Stefan Thiel, German Hammerl, Jochen Mannhart, and Jean-Marc Triscone. 2008. "Electric field control of the LaAlO3/SrTiO3 interface ground state." *Nature* 456 (7222): 624–27. https://doi.org/10.1038/nature07576.

Electric field control of the $LaAlO_3/SrTiO_3$ interface ground state

A. D. Caviglia[1], S. Gariglio[1], N. Reyren[1], D. Jaccard[1], T. Schneider[2], M. Gabay[3], S. Thiel[4], G. Hammerl[4], J. Mannhart[4] & J.-M. Triscone[1]

Interfaces between complex oxides are emerging as one of the most interesting systems in condensed matter physics[1]. In this special setting, in which translational symmetry is artificially broken, a variety of new and unusual electronic phases can be promoted[2]. Theoretical studies predict complex phase diagrams and suggest the key role of the charge carrier density in determining the systems' ground states. A particularly fascinating system is the conducting interface between the band insulators $LaAlO_3$ and $SrTiO_3$ (ref. 3). Recently two possible ground states have been experimentally identified: a magnetic state[4] and a two-dimensional superconducting condensate[5]. Here we use the electric field effect to explore the phase diagram of the system. The electrostatic tuning of the carrier density allows an on/off switching of superconductivity and drives a quantum phase transition[6–8] between a two-dimensional superconducting state and an insulating state. Analyses of the magnetotransport properties in the insulating state are consistent with weak localization and do not provide evidence for magnetism. The electric field control of superconductivity demonstrated here opens the way to the development of new mesoscopic superconducting circuits.

Since the discovery of conductivity at the $LaAlO_3/SrTiO_3$ interface, one of the main challenges has been the identification of the source of charge carriers. Despite much research effort[9–12] there is not yet a general consensus on the nature of the doping mechanism. Depending on the growth conditions, the doping can be related to the polar nature of the $LaAlO_3$ atomic planes[13] (the polar catastrophe model or 'intrinsic doping'), to the creation of oxygen defects during the growth of the samples[9–11] or to interdiffusion phenomena[12] ('extrinsic doping'). It is generally accepted that the conduction observed in samples grown at low oxygen pressure (less than about 10^{-6} mbar) is dominated by oxygen defects and extends deeply into the substrate, whereas for samples grown at higher pressure (over about 10^{-5} mbar) the conduction is confined to the interface[14]. Both superconductivity[5] and unusual magnetotransport properties, attributed to magnetism[4], have recently been observed in samples grown in the high-pressure regime. These results suggest that the ground state of the system might be sensitive to small changes in carrier concentration, or to the amount of disorder, or both. To resolve this issue and investigate the phase diagram of the system, electrostatic doping seems to be an ideal technique, because it allows the tuning of the carrier density while preserving the oxygen concentration and disorder landscape[15,16]. Recent reports indicate that an electric field can effectively modulate the transport properties of the $LaAlO_3/SrTiO_3$ interface[17].

$LaAlO_3/SrTiO_3$ superconducting interfaces and field-effect devices were prepared as described in the Methods. In a standard field-effect device, an electric field is applied between a metallic gate and a conducting channel across a dielectric. We used the 0.5-mm-thick $SrTiO_3$ substrate as the dielectric because it is characterized at low temperatures by a large dielectric constant. The metallic gate is a gold film sputtered opposite to the channel area onto the back of the substrate. In this configuration the electric field modulates the concentration of carriers in the interface conducting channel. A sketch of the field-effect device is shown in Fig. 1.

To quantify the carrier density modulation resulting from the field effect, the electric field dependence of the $SrTiO_3$ permeability needs to be taken into account[18]. We therefore measured the differential capacitance $C(V) = \mathrm{d}Q(V)/\mathrm{d}V$ of the device as a function of the applied gate voltage V, $Q(V)$ being the induced charge. Charge trapping can occur in $SrTiO_3$ and may cause the appearance of hysteresis in the $C(V)$ measurements[19]. Indeed, we found that the capacitance depended on the voltage sweep history. However, the devices present reversible and reproducible $C(V)$ characteristics when the field is first ramped to the highest positive voltage. Following this experimental procedure, the field-induced modulation of charge density δn_{2D} between gate voltages V_1 and V_2 can be evaluated using the relation

$$\delta n_{2D} = \frac{1}{Se}\int_{V_1}^{V_2} C(V)\mathrm{d}V \qquad (1)$$

where S is the area of the gate electrode and e is the elementary charge. The $C(V)$ characteristic of a device made of a layer of $LaAlO_3$ nine unit

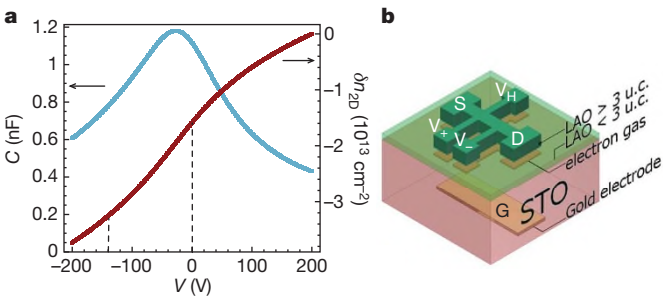

Figure 1 | Dielectric characterization of the field-effect device. a, Dielectric tunability of the differential capacitance (C versus V) measured on a device at 1.5 K (blue). The capacitance $C(V)$ is measured with an a.c. technique applying a signal amplitude of 1 V. Change in the 2D carrier concentration as a function of gate voltage is calculated using equation (1) with $V_1 = 200$ V and $V_2 = V$ (red). The dashed lines indicate the region where the quantum critical behaviour is observed. Note that in this region $\delta n_{2D} \propto \delta V$. **b**, Schematic view of a field-effect device, showing the source (S), drain (D), longitudinal voltage (V_+ and V_-), Hall voltage (V_H) and gate voltage (G) contacts. STO, $SrTiO_3$; LAO, $LaAlO_3$.

[1]Département de Physique de la Matière Condensée, University of Geneva, 24 Quai Ernest-Ansermet, 1211 Genève 4, Switzerland. [2]Physikinstitut, University of Zurich, Winterthurerstrasse 190, 8057 Zurich, Switzerland. [3]Laboratoire de Physique des Solides, Bat 510, Université Paris-Sud 11, Centre d'Orsay, 91405 Orsay Cedex, France. [4]Experimental Physics VI, Center for Electronic Correlations and Magnetism, Institute of Physics, University of Augsburg, D-86135 Augsburg, Germany.

cells thick, and the corresponding modulation of carrier density, are presented in Fig. 1a. The carrier concentration of the as-grown sample has been measured using the Hall effect ($n_{2D} \approx 4.5 \times 10^{13}\,\mathrm{cm}^{-2}$ at 100 K). The maximum modulation of the carrier density that was achieved is remarkably close to the total number of free carriers present in the system, indicating that the electric field effect is an excellent tool to probe its phase diagram. On the same sample we measured the temperature dependence of the sheet resistance R_{sheet} for various gate voltages V.

Figure 2a shows the sheet resistance as a function of temperature for applied gate voltages between −300 V and 320 V; Fig. 2b displays the same data on a linear sheet-resistance scale. This behaviour has been observed in several samples. A variation of the gate voltage induces a large modulation of the normal-state resistance, which changes by two orders of magnitude, and a remarkable tuning of the superconducting critical temperature. For large negative voltages, corresponding to the smallest accessible electron densities, the sheet resistance increases as the temperature is decreased, indicating an insulating ground state (conductance $G \to 0$ as $T \to 0$). As the electron density is increased the system becomes a superconductor. The transition from superconducting to insulating ground state occurs at a critical sheet resistance of $R_c \approx 4.5\,\mathrm{k\Omega}$ per square, close to the quantum of resistance for bosons with charge $2e$, $R_Q = h/4e^2 \approx 6.45\,\mathrm{k\Omega}$. A further increase in the electron density produces first a rise of the critical temperature to a maximum of ~310 mK. For larger voltages, the critical temperature decreases again, providing evidence for an overdoped regime. These measurements thus reveal the existence of a quantum phase transition between a superconducting and an insulating phase at the $LaAlO_3/SrTiO_3$ interface and demonstrate that the ground state of the system depends on its carrier density.

Close to the critical point, the sheet resistance measured at 400 mK shows a remarkable phenomenon. As can be seen in Fig. 3, approaching the quantum critical point from the superconducting region of the phase diagram, a linear dependence of the sheet resistance as a function of the applied voltage is observed. Once the critical point has been crossed, however, a further reduction of carrier concentration produces a much steeper variation in resistance.

To establish the critical temperature versus carrier density phase diagram, a criterion to define the critical temperature for each gate voltage is needed. It has been shown that the superconducting transitions are consistent with the Berezinskii–Kosterlitz–Thouless (BKT)

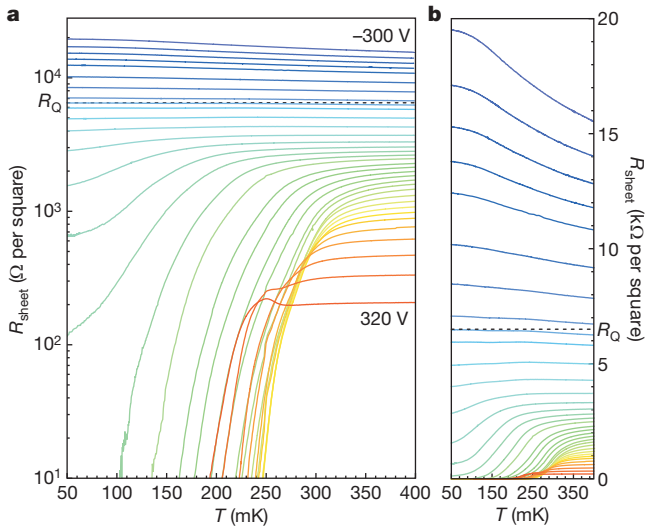

Figure 2 | Field-effect modulation of the transport properties. a, Measured sheet resistance as a function of temperature, plotted on a semi-logarithmic scale, for gate voltages varying in 10-V steps between −300 V and −260 V, 20-V steps between −260 V and 320 V, and for −190 V. The dashed line indicates the quantum of resistance R_Q. **b**, The same data plotted on a linear resistance scale.

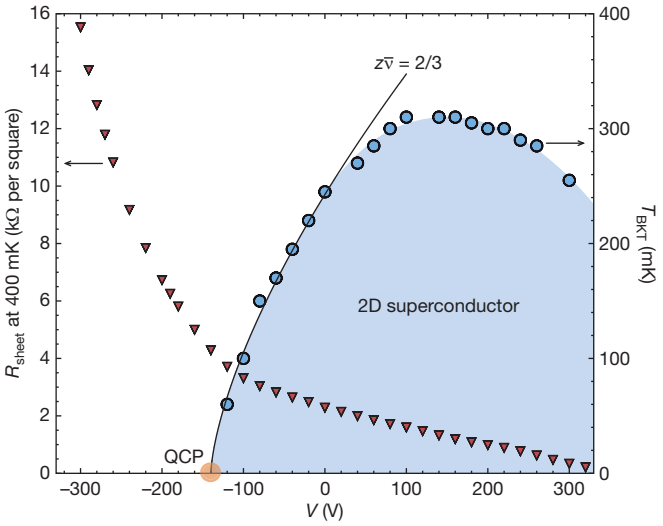

Figure 3 | Electronic phase diagram of the $LaAlO_3/SrTiO_3$ interface. Critical temperature T_{BKT} (right axis, blue dots) is plotted against gate voltage, revealing the superconducting region of the phase diagram. The solid line describes the approach to the quantum critical point (QCP) using the scaling relation $T_{\mathrm{BKT}} \propto (V - V_c)^{z\bar{\nu}}$, with $z\bar{\nu} = 2/3$. Also plotted is normal-state sheet resistance, measured at 400 mK (left axis, red triangles) as a function of gate voltage.

behaviour expected for a two-dimensional system[5]. According to the BKT model, above the critical temperature T_{BKT} the temperature dependence of the resistance is expected to be

$$R \propto \exp\left(-\frac{b_R}{(T - T_{\mathrm{BKT}})^{1/2}}\right) \qquad (2)$$

where b_R is a parameter related to the vortex properties.

This approach allows T_{BKT} to be extracted for each applied gate voltage and the phase diagram to be mapped. The result is shown in Fig. 3. Reducing the carrier concentration from the largest doping level ($V = 320$ V), T_{BKT} first increases, reaches a maximum at around 310 mK and then decreases to zero. This critical line ends at $V_c \approx -140$ V, where the system undergoes a quantum phase transition (QPT).

To investigate the quantum critical region in detail we consider a continuous QPT separating a superconducting ground state and an insulating ground state. The control parameter of the phase transition is the variation of the carrier concentration $\delta n_{2D} = n_{2D} - n_{2Dc}$, where n_{2Dc} is the sheet carrier density at the critical point. Figure 1a shows a quasi-linear relationship between the applied gate voltage and the variation of carrier concentration $\delta n_{2D} \propto \delta V = V - V_c$ near the critical point. Hence we can use the gate voltage as the tuning parameter for the analysis of the QPT. For a continuous QPT, the quantum critical region is characterized by a spatial and a temporal correlation length that diverge respectively as $\xi \propto (\delta n_{2D})^{-\bar{\nu}}$ and $\xi_\tau \propto (\delta n_{2D})^{-\nu_\tau}$. The quantum dynamic critical exponent is defined through the ratio $z = \nu_\tau/\bar{\nu}$. According to the scaling theory of quantum critical phenomena[20–22] the phase transition line $T_{\mathrm{BKT}}(\delta V)$ presented in Fig. 3 is expected to scale, near the quantum critical point, as

$$T_{\mathrm{BKT}} \propto (\delta n_{2D})^{z\bar{\nu}} \propto (\delta V)^{z\bar{\nu}} \qquad (3)$$

In Fig. 3 we observe that the approach to quantum criticality is well described by $z\bar{\nu} = 2/3$, exponents that also describe well $T_{\mathrm{BKT}} \propto (\delta n_{2D})^{z\bar{\nu}}$. We note that the product $z\bar{\nu} = 2/3$ agrees with the results obtained in previous studies of two-dimensional (2D) quantum superconductor to insulator phase transitions driven by magnetic and electric fields in amorphous bismuth films[23] and $Nb_{0.15}Si_{0.85}$ films[24]. The value $z\bar{\nu} = 2/3$ is compatible with the 3D-XY model[6],

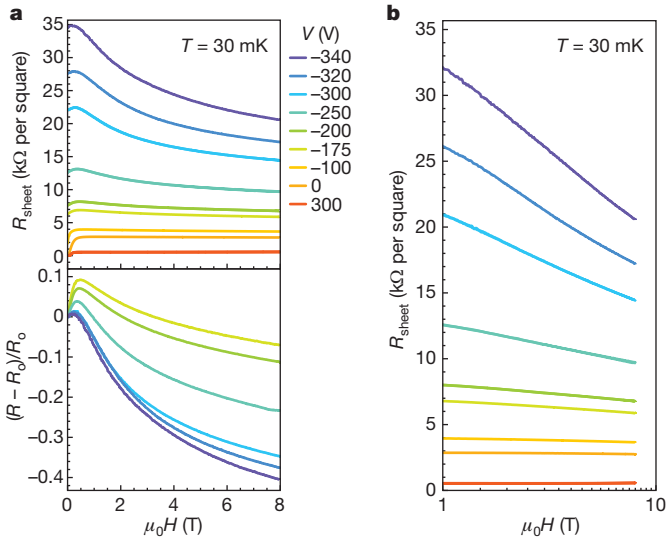

Figure 4 | Field-effect modulation of the magnetotransport properties. **a**, Sheet resistance (upper panel) and magnetoresistance (lower panel), as a function of magnetic field, measured for different gate voltages at 30 mK. Note the large negative magnetoresistance for the lowest carrier densities. **b**, Sheet resistance as a function of magnetic field, measured for different gate voltages at 30 mK and plotted on a logarithmic magnetic field scale.

possibly indicative of a clean (or weakly disordered) 2D system in which quantum fluctuations dominate ((2+1)D-XY). The voltage range over which critical fluctuations can be observed has, however, to be determined. We note that a highly disordered (dirty boson) system[25] with localized Cooper pairs in the insulating phase would yield $z\bar{\nu} = 1$. This value would agree with the critical behaviour observed in $NdBa_2Cu_3O_{7-\delta}$ thin films[26]. Although the dirty boson interpretation is not incompatible with the data, in most systems dominated by disorder the magnetoresistance is expected to be positive, at variance with our observations (see below).

Of particular relevance for the understanding of the nature of this electronic system is the insulating region of the phase diagram. In the accessible temperature range the variation of the conductance can be explained by weak localization[27,28]. Figure 4a depicts the dependence of the sheet resistance in a perpendicular magnetic field measured at 30 mK. As expected if weak localization is governing the magnetotransport properties, we observe a large negative magnetoresistance that increases as we move more deeply into the insulating phase, reaching more than −40% at 8 T for the lowest measured carrier concentration. Above ∼1 T the resistance decreases logarithmically with increasing magnetic field (Fig. 4b). In the non-superconducting region of the phase diagram no hysteresis in magnetoresistance has been detected (see also Methods). Our data are in partial agreement with the results presented in ref. 4, where a negative magnetoresistance was also reported.

The field-effect tuning of the electronic properties of the $LaAlO_3$/$SrTiO_3$ interface achieved here unravels a complex phase diagram controlled by the charge density with a quantum critical point separating a superconducting and an insulating region. Using the electrostatic control of superconductivity, new quantum electronic devices can be envisaged where, for instance, superconductivity can be dynamically defined and controlled using local electric fields.

METHODS SUMMARY

We prepared conducting interfaces by depositing $LaAlO_3$ films, with thickness more than four unit cells, on TiO_2-terminated (001) $SrTiO_3$ single crystals. The films were grown by pulsed laser deposition at ∼800 °C in $\sim 1 \times 10^{-4}$ mbar of O_2 with a repetition rate of 1 Hz. The fluence of the laser pulses was 0.6 J cm^{-2}. We monitored film growth *in situ* using reflection high-energy electron diffraction which allowed the thickness to be controlled with sub-unit-cell precision[29]. After growth, each sample was annealed in 200 mbar of O_2 at about 600 °C for one hour and cooled to room temperature in the same oxygen pressure. Samples with different thickness of $LaAlO_3$ were systematically characterized using atomic force microscopy and X-ray diffraction. The samples were then patterned in a geometry suitable for four-point transport measurements. The patterning technique is based on the discovery that only regions covered by a $LaAlO_3$ layer with thickness ≥4 unit cells are conducting[17]. The $LaAlO_3$ thickness was thus reduced to about two unit cells or less in specific regions of the samples, irradiating them with argon ions while protecting transport channels with a photoresist layer. The superconducting interface was contacted by ultrasonic welding using Al-wires. Transport properties were measured in a dilution cryostat applying a linear current density of 2×10^{-4} A m^{-1} in a 500-μm-wide path. Magnetic fields were applied perpendicular to the sample and ramped with a sweep rate of 1.6 mT s^{-1}. Higher sweep rates (3.2 mT s^{-1}) revealed, in the superconducting region of the phase diagram, small hystereses (1%) in the magnetoresistance. Such hystereses were not observed in the insulating region. Electric fields were applied using a voltage source. No leakage currents (≤1 nA) could be detected up to the largest applied voltages. The devices present reversible and reproducible $C(V)$ characteristics when the field is first ramped to the highest positive voltage. Note that in our experimental procedure the 0 V state does not correspond to the as-grown state. The maximum applied electric field was chosen to avoid any breakdown of the electrical insulation inside the dilution cryostat.

1. Hwang, H. Y. Atomic control of the electronic structure at complex oxide heterointerfaces. *Mater. Res. Soc. Bull.* **31,** 28–35 (2006).
2. Okamoto, S. & Millis, A. J. Electronic reconstruction at an interface between a Mott insulator and a band insulator. *Nature* **428,** 630–633 (2004).
3. Ohtomo, A. & Hwang, H. Y. A high-mobility electron gas at the $LaAlO_3$/$SrTiO_3$ heterointerface. *Nature* **427,** 423–426 (2004).
4. Brinkman, A. *et al.* Magnetic effects at the interface between non-magnetic oxides. *Nature Mater.* **6,** 493–496 (2007).
5. Reyren, N. *et al.* Superconducting interfaces between insulating oxides. *Science* **317,** 1196–1199 (2007).
6. Sachdev, S. *Quantum Phase Transitions* (Cambridge Univ. Press, 1999).
7. Sondhi, S. L., Girvin, S. M., Carini, J. P. & Shahar, D. Continuous quantum phase transitions. *Rev. Mod. Phys.* **69,** 315–333 (1997).
8. v. Löohneysen, H., Rosch, A., Vojta, M. & Wölfle, P. Fermi-liquid instabilities at magnetic quantum phase transitions. *Rev. Mod. Phys.* **79,** 1015–1075 (2007).
9. Herranz, G. *et al.* High mobility in $LaAlO_3$/$SrTiO_3$ heterostructures: origin, dimensionality, and perspectives. *Phys. Rev. Lett.* **98,** 216803 (2007).
10. Kalabukhov, A. *et al.* Effect of oxygen vacancies in the $SrTiO_3$ substrate on the electrical properties of the $LaAlO_3$/$SrTiO_3$ interface. *Phys. Rev. B* **75,** 121404 (2007).
11. Siemons, W. *et al.* Origin of charge density at $LaAlO_3$ on $SrTiO_3$ heterointerfaces: Possibility of intrinsic doping. *Phys. Rev. Lett.* **98,** 196802 (2007).
12. Willmott, P. R. *et al.* Structural basis for the conducting interface between $LaAlO_3$ and $SrTiO_3$. *Phys. Rev. Lett.* **99,** 155502 (2007).
13. Nakagawa, N., Hwang, H. Y. & Muller, D. A. Why some interfaces cannot be sharp. *Nature Mater.* **5,** 204–209 (2006).
14. Basletic, M. *et al.* Mapping the spatial distribution of charge carriers in $LaAlO_3$/$SrTiO_3$ heterostructures. *Nature Mater.* **7,** 621–625 (2008).
15. Ahn, C. H., Triscone, J.-M. & Mannhart, J. Electric field effect in correlated oxide systems. *Nature* **424,** 1015–1018 (2003).
16. Ahn, C. H. *et al.* Electrostatic modification of novel materials. *Rev. Mod. Phys.* **78,** 1185–1212 (2006).
17. Thiel, S., Hammerl, G., Schmehl, A., Schneider, C. W. & Mannhart, J. Tunable quasi-two-dimensional electron gases in oxide heterostructures. *Science* **313,** 1942–1945 (2006).
18. Matthey, D., Gariglio, S. & Triscone, J.-M. Field-effect experiments in $NdBa_2Cu_3O_{7-\delta}$ ultrathin films using a $SrTiO_3$ single-crystal gate insulator. *Appl. Phys. Lett.* **83,** 3758–3760 (2003).
19. Christen, H.-M., Mannhart, J., Williams, E. J. & Gerber, C. Dielectric properties of sputtered $SrTiO_3$ films. *Phys. Rev. B* **49,** 12095–12104 (1994).
20. Schneider, T. Universal critical quantum properties of cuprate superconductors. *Acta Phys. Polon. A* **91,** 203–212 (1997).
21. Schneider, T. *The Physics of Superconductors* Vol. 2, 111 (Springer, 2004).
22. Schneider, T. & Singer, J. M. *Phase Transition Approach to High Temperature Superconductivity* (Imperial College Press, 2000).
23. Parendo, K. A. *et al.* Electrostatic tuning of the superconductor–insulator transition in two dimensions. *Phys. Rev. Lett.* **94,** 197004 (2005).
24. Aubin, H. *et al.* Magnetic-field-induced quantum superconductor–insulator transition in $Nb_{0.15}Si_{0.85}$. *Phys. Rev. B* **73,** 094521 (2006).
25. Fisher, M. P. A. & Grinstein, G. Quantum critical phenomena in charged superconductors. *Phys. Rev. Lett.* **60,** 208–211 (1988).
26. Matthey, D., Reyren, N., Schneider, T. & Triscone, J.-M. Electric-field-effect modulation of the transition temperature, mobile carrier density, and in-plane penetration depth of $NdBa_2Cu_3O_{7-\delta}$ thin films. *Phys. Rev. Lett.* **98,** 057002 (2007).

27. Bergmann, G. Weak localization in thin films. *Phys. Rep.* **107,** 1–58 (1984).
28. Das, D. & Doniach, S. Weakly localized bosons. *Phys. Rev. B* **57,** 14440–14443 (1998).
29. Rijnders, G., Koster, G., Blank, D. H. A. & Rogalla, H. In situ monitoring during pulsed laser deposition of complex oxides using reflection high energy electron diffraction under high oxygen pressure. *Appl. Phys. Lett.* **70,** 1888–1890 (1997).

Acknowledgements We thank T. Giamarchi, L. Benfatto, T. Kopp and A.-S. Ruetschi for discussions and M. Lopes for technical assistance. We acknowledge financial support by the Swiss National Science Foundation through the National Centre of Competence in Research 'Materials with Novel Electronic Properties' MaNEP and Division II, by the European Union through the project 'Nanoxide', by the Deutsche Forschungsgemeinschaft through the SFB484, and by the European Science Foundation through the program 'Thin Films for Novel Oxide Devices'.

Author Information Reprints and permissions information is available at www.nature.com/reprints. Correspondence and requests for materials should be addressed to A.D.C. (andrea.caviglia@unige.ch.).